Available online at www.sciencedirect.com

Chemical Engineering Research and Design

journal homepage: www.elsevier.com/locate/cherd

Chemical modification of reduced graphene oxide membranes: Enhanced desalination performance and structural properties for forward osmosis

Mohamed Edokali[a], *Rachel Bocking*[b], *Mozhdeh Mehrabi*[a], *Alexander Massey*[b], *David Harbottle*[a], *Robert Menzel*[b], *Ali Hassanpour*[a,*]

[a] *School of Chemical and Process Engineering, Faculty of Engineering and Physical Science, University of Leeds, Leeds LS2 9JT, UK*

[b] *School of Chemistry, Faculty of Engineering and Physical Science, University of Leeds, Leeds LS2 9JT, UK*

ARTICLE INFO

Article history:
Received 4 August 2023
Received in revised form 2 October 2023
Accepted 8 October 2023
Available online 10 October 2023

Keywords:
Reduced graphene oxide
Polyetheneimine
Polydopamine
Forward osmosis
Desalination membrane
Dimensional stability

ABSTRACT

Graphene oxide (GO) nanosheets can offer a breakthrough into the development of novel and efficient laminated forward osmosis membranes, with high hydrophilicity and outstanding desalination performance. However, fabrication of desirable GO-based nanocomposite membrane which can overcome the on-going trade-off between forward osmosis (FO) performance and chemical/mechanical stability, remains to be challenging in practical application. In this study, polyethyleneimine (PEI) was used to reduce GO (rGO) and crosslink and surface modify membrane's GO sheets for the performance enhancement. The crosslinked rGO was then deposited on a hydrophilic nylon support layer (modified by polydopamine, pDA, for structural stability) using vacuum filtration method. The resulting PEI:rGO/pDA membrane showed excellent water flux (25.5 LMH), high sodium chloride (NaCl) salt rejection (98.9%), and low reverse solute flux (0.91 gMH) in lab-scale tests. The combination of crosslinking GO with PEI and modifying the support layer with polydopamine (pDA) enhanced the membranes hydrophilicity and structural stability. The incorporation of PEI into GO resulted in compacted nanochannels, improving molecular/ions separation. Moreover, the pDA coating enhanced desalination performance and reduced internal concentration polarisation effects, further improving the membrane durability and integrity through the formation of numerous binding sites for firmly anchoring with the PEI:rGO nanocomposite structure.

1. Introduction

Water shortage and demand have recently become particularly challenging with the increasing of the global population. Membrane-based water treatment and purification technologies have shown excellent potentials for recovery and supply of clean water from sea and waste waters (Castelletto and Boretti, 2021; Li et al., 2020; Wu et al., 2020). However, the conventional hydraulically driven methods, including nanofiltration (NF) and reverse osmosis (RO), have generally encountered high energy consumption issues and severe membrane fouling (McCutcheon and Elimelech, 2006).

Forward osmosis (FO), an emerging water treatment-based technology, has been considered as one of the most efficient methods for seawater desalination, with the potential of low energy requirements for its operational

* Corresponding author.
E-mail address: A.Hassanpour@leeds.ac.uk (A. Hassanpour).

https://doi.org/10.1016/j.cherd.2023.10.022

application (Goh et al., 2016; Akther et al., 2015). Forward osmosis (FO) for water desalination is mainly driven by the difference in the osmotic pressure (i.e., chemical potentials) between two solutions of different concentrations permeated counter-currently across a semipermeable membrane (Cath et al., 2006). However, the practical application of FO desalination still suffers from several challenges, including low water flux, reverse solute flux, membrane fouling, and severe internal concentration polarisation (ICP) (Zhao et al., 2012). These challenges are mainly reported for the use of few types of commercially available polymeric membranes in FO process, which lowers the desalination performance (Akther et al., 2015; Ndiaye et al., 2019). Therefore, this has led to an urgent need for the development of novel membrane materials for improved FO performance for water desalination.

Recently, graphene oxide (GO) nanosheets have received an immense attention for the development of next-generation of water-based laminar membranes for desalination, specifically in FO process (Yan et al., 2017a). GO nanosheets, as water purification membrane materials, possess unique properties, including abundant of negatively charged oxygen-containing functional groups (e.g., epoxy, hydroxyl, carbonyl, and carboxyl), high hydrophilicity, high mechanical and chemical stability, and atomic-like thickness (Stankovich et al., 2007; Huang et al., 2014). GO nanosheets can be stacked in a layered structure (with nanochannels or d-spacing) to fabricate water purification membranes, using various methods, such as vacuum-assisted filtration, layer-by-layer, drop-casting, spin-coating, and electrophoretic deposition (Han et al., 2013; Hu and Mi, 2013; Kim et al., 2013; Fan et al., 2019). The nano-channels can play a crucial role in enhancing water transport and molecular selectivity of ions through low-friction passages in the GO membrane (Song et al., 2019). However, the instability of GO stacked laminates remains problematic when exposed to aqueous solutions, which can lead to loosen the structure of GO and thus deteriorating its rejection performance towards monovalent ions (e.g., Na^+) in desalination applications (Abraham et al., 2017; Zheng et al., 2017; Zhang and Chung, 2017). The issue of low dimensional stability mainly occurs due to the destruction of hydrogen bonding between oxygen-functional groups of GO laminates, as a result of hydration effects (Kim et al., 2017). To resolve this issue in the desalination field, researchers have developed feasible strategies to tune the d-spacing of GO laminates and prepare more stable GO membranes by crosslinking or reduction to support substrate of GO nanosheets. However, the molecular sieving performance and water permeability of the modified GO membranes may be hindered by extremely narrowing the nanochannels and uncontrolled loading of crosslinkers. Therefore, the procedure of tuning the d-spacing between GO nanosheets should be carefully considered according to application fields (Castelletto and Boretti, 2021; Wu et al., 2020; Johnson and Hilal, 2020).

In particular, the performance of GO-based laminar FO membranes for desalination was found to be greatly dependent on the microstructure characteristics of GO nanosheets (Tiwari et al., 2019). The swelling phenomenon of GO laminates in FO desalination membranes has been reported to be controlled by assembling and modifying GO nanosheets with different metals and their oxides, such as propanedioic acid (PPA) (Yan et al., 2017b), metal-organic framework (MOF) (Pang et al., 2019), polystyrene sulfonic acid (PSS) (Deka et al., 2021), layered double hydroxides (LDHs) (Wang et al., 2022), potassium chloride (KCl) (Talar et al., 2019), *N*-isopropylacrylamide (NIPAM) (Kim et al., 2017), or even chemically reduced by Hydriodic acid (HI) (Fan et al., 2019; Yang et al., 2017, 2018). Although, each study has a certain target, for example increasing water permeation, salt rejection, studies that address simultaneous improvement of a set of performance and stability parameters are rare, to the best of our knowledge. Yu et al (Wu et al., 2020). recently reported that there is still an urgent need to search for more effective crosslinkers for performance enhancement of GO laminar membranes since the practical application of FO desalination mainly involves mechanical and chemical washing procedures for membrane recovery. Therefore, it would be of great scientific interests to develop effective approaches for the fabrication of promising GO laminar FO membranes to overcome the on-going trade-off between the desalination performance and long-term physical and chemical stability.

In this study, the challenges for employing GO membranes in FO desalination were attempted to be addressed using two technical facile approaches. Initially, GO laminates were chemically crosslinked, reduced and modified, simultaneously, by in situ incorporation of branched polyethyleneimine (PEI) molecules with a low controlled concentration. Branched PEI is an organic candidate which contains a variety of amino functional groups (i.e., $-NH_2R$, NHR_2, and $-NR_3$), forming a potential source for nitrogen and carbon elements (Zhou et al., 2015; Zhang et al., 2015). The advantages of branched PEI was successfully employed, as reducing agent, hydrophilic surface modifier and polymer crosslinker, to prepare reduced graphene oxide (rGO) membranes for gas purification applications (Aghehrochaboki et al., 2019; Liu et al., 2013; Li et al., 2019a). PEI was used as a hydrophilic surface modifer of GO membrane (Jia and Wang, 2015) for the RO application, but to the best of our knowledge, the direct functionalisation process of branched PEI into GO sheets as crosslinker, reducing agent and surface modifer has not been reported for the fabrication of water treatment, purification and FO membranes. Herein, this role was proposed to partially remove the oxygen-containing functional groups from GO dispersion, provide crosslinking route of PEI-based amine functional groups to the carboxylic and epoxyl groups of GO nanosheets, and provide anchor sites for addition of hydrophilic nanomaterials for FO-GO desalination membranes. Consequently, the d-spacing between rGO laminates can be narrowed, which could be ideal to enhance the stability of GO laminates in aqueous solutions and improve rejection efficiency towards ionic species for desalination (Jang et al., 2020). The second step involved the coating of the as-synthesised polydopamine (pDA) onto the nylon substrate to improve the hydrophilicity of support substrate and generate feasible modification sites to improve the adhesion between nylon substrate and PEI doped rGO layers that shall be deposited using vacuum-assisted filtration onto the surface of pDA coated nylon membrane. The pDA is an abundantly amino-contained polymer substance, with adhesive-inspired property, which has been widely used to enhance the wettability of membranes and provide feasibly adhesion between support substrates and the GO layers (Yang et al., 2017; Zhang et al., 2015). The pDA can significantly contribute to enhance the dimensional stability of PEI functionalised rGO film, water permeation, salt rejection efficiency, and reverse solute flux reduction, compared to PEI:rGO deposited on a pristine nylon substrate. In this

work, the physico-chemical and morphological properties of as-synthesised functionalised materials and membranes were studied. Moreover, the desalination performance, in terms of water flux, reverse solute flux, selectivity and salt rejection, of the synthesised rGO laminar membranes was assessed in a lab-scale FO process, and was compared to that of pDA modified GO (*as a reference membrane*) and commercial cellulose triacetate (CTA)-FO membranes. The structural integrity and durability of synthesised membranes in harsh conditions and chemical solutions were also investigated. This study can offer insight for the fabrication of highly stable rGO-based laminar FO membranes with excellent desalination performance.

2. Experimental

2.1. Materials

Graphene oxide dispersion (with a stock concentration of 1.03%, 10 mg/mL, pH ≤ 2, variable sheet size) was provided by William Blythe Ltd. The following chemicals were purchased from different suppliers as follows: Branched polyethyleneimine (99%, M.W: 25 k, Sigma-Aldrich), dopamine hydrochloride (98%, Sigma-Aldrich), hydrochloric acid (37%, 1M, VWR international Ltd), Tris(hydroxymethyl)aminomethane (Tris base salt, 219–220°C/ 10 mmHg, Fluorochem Limited, sodium chloride (M.W: 58.44 g/mol, VWR international Ltd), dextrose (M.W: 180.16 g/mol, Alfa Aesar). Commercial Nylon 6, 6 support substrates (diameter: 47 mm, pore size: 0.2 µm, porosity: 70 – 85%, thickness:~ 80 µm), and commercial FTSH2O Cellulose Triacetate flat sheet (porosity:~ 70%, thickness:~ 50 µm) membranes were purchased from STERLITECH corporation. Ethanol (≥ 70% v/v) and sodium hypochlorite (≥ 10% chlorine, M.W: 74.44 g/mol) were provided by Scientific Laboratory Supplies (SLS). Deionised water (DIW, 18.3 MΩ/cm, 25 °C, Millipore system) was used throughout the work to prepare all aqueous solutions. All chemicals and materials were used as reagent grades without any further purification.

2.2. Methods

2.2.1. Synthesis of PEI:rGO dispersions

The preparation process of PEI:rGO/pDA laminar membranes is schematically shown in **scheme (S1)**. In particular, the synthesis of PEI:rGO laminates was initially involved the dispersion of pristine GO into DI water with an optimised concentration (see **Section S2, SI**) under a vigorous stirring (Asynt, ADS-HP-NT hotplate stirrer) at 830 rpm for 5 min. The GO dispersion was then subjected to ultrasonication (BRANSONIC 2800-E CPX ultrasonic water bath) for 15 min to obtain monolayer GO sheets. Subsequently, the resultant dispersed GO was added drop wise into controlled amounts of branched PEI solution, with PEI:GO feeding ratios of 0.01:1 (*0.01 wt/wt%*), 0.1:1 (*0.1 wt/wt%*) and 1:1 (*1 wt/wt%*), under continuous stirring and followed by ultrasonication for 15 min at ambient temperature. The obtained PEI:GO mixture was transferred into the round-bottom-flask (RBF) and refluxed under a vigorous stirring (760 rpm) at 80 °C for 2 h, at which the colour of the mixture was transformed from brown into black, conforming the formation of rGO dispersion. The synthesised PEI:rGO dispersion was then subjected to centrifuge (ThermoFisher Scientific, Megafuge™ R16 Centrifuge Series) at 10,000 rpm for 30 min, and the supernatant, which contained residual multi-layered PEI:rGO particles, was fully discarded. The resultant product was freeze-dried (LABCONCO FreeZone Benchtop Freeze Dryer) at – 50 °C for 5 days to yield blackish/greenish coloured sheets compared to blackish/greyish pure GO sheets, as shown in **Fig. (S1)**.

2.2.2. Preparation of PEI:rGO/pDA layered membranes

The resultant freeze-dried PEI:rGO products were then dispersed in DI water by further sonication and vigorously stirring for 1 h to prepare homogenous solutions for membrane fabrication. Here, the choice of a nylon substrate for membrane fabrication was attributed to its intrinsic hydrophilicity, highly porous fibrous network, and excellent mechanical stability. Additionally, its structural/transport parameters compared to commercial FO membranes minimizes the ICP effects, a key concern in FO processes (Kim et al., 2017; Fernández-Márquez et al., 2022; Jusoh et al., 2019; Huang et al., 2013a). Prior to the filtration process of the PEI:rGO membrane with an optimised feeding ratio of 0.01:1 **(Section S2, SI)**, the nylon substrate was modified with polydopamine (pDA) to further enhance its hydrophilicity and improve its interfacial adhesion with PEI:rGO (with an optimum concentration of 0.01 wt/wt%) active layer (*denote as PEI:rGO/pDA*). The pDA coating solution (with a controlled concentration of 0.5 mg/mL) was prepared by dissolving 0.005 g of dopamine hydrochloride into 10 mL of as-prepared 0.01 M Tris-HCL buffer (pH 8.5) for 30 min (*synthesis process of Tris-buffer is addressed* in **section (S3, SI)**). It is worth noting that the pDA particles can be easily formed by the self-polymerisation of DA in highly active alkaline conditions at the pH level of 8.5. The nylon substrates were then dipped in the as-prepared pDA solution under a room temperature for an optimum period of 1.5 h **(Section S4, SI)** to undergo self-polymerisation and form anchor sites for adhesion of PEI:rGO deposited layer. Subsequently, the substrates were harshly rinsed with DI water for five times to remove excess of pDA solution. To prepare optimised PEI: rGO framework membrane, different amounts (i.e., 2, 4, and 6 mL) of the obtained stable dispersion were vacuum filtered (with a speed of ~ 0.2 mL/min) on the pDA modified nylon substrates to self-assemble PEI: rGO sheets during the filtration process using an in-house built filtration device. After harsh rinsing with DI water, the as-fabricated PEI:rGO/pDA film was kept in a desiccator for 24 h for an initial drying. Then, the resultant membrane was dried in a vacuum oven (GALLENKAMP Fistreem vacuum oven) at 50 °C for 2.5 h. The dried membrane was finally stored in a desiccator for further characterisations and FO performance tests. In addition, PEI:rGO dispersion was deposited on a non-modified pristine nylon support layer for further evaluation and analysis (*denote as PEI:rGO*). For better comparisons with PEI:rGO membranes, pristine GO solutions were similarly vacuum filtered onto the pristine and pDA-modified nylon substrates (*denoted as GO and GO/pDA membranes*), respectively. The schematic for formulation process of membranes, at which the GO-based laminar membranes were prepared, are summarised in Table (1).

2.3. Material and membrane characterisation

Physicochemical and morphological properties of the PEI functionalised rGO materials and membranes, compared to that for GO, were initially characterised by using different analytical techniques. Surface chemistry and chemical

Table 1 – Formulation and modelled framework structures of the resultant GO-based composite membranes.

Membrane	Denotation	Modelled Structure
GO deposited on a pristine nylon substrate	**GO**	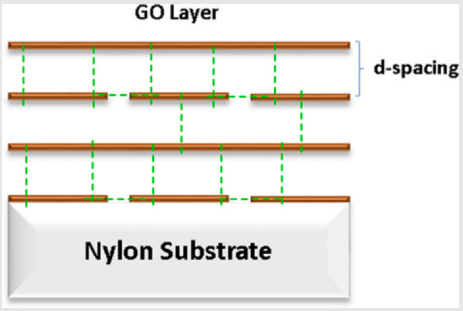
GO deposited on a pDA modified nylon substrate	**GO/pDA**	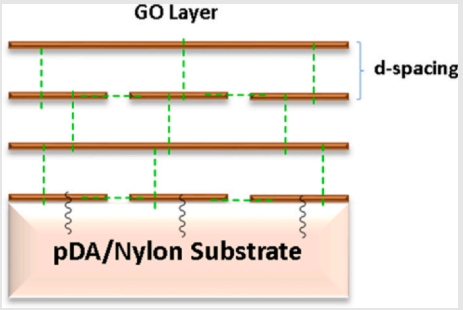
PEI:rGO deposited on a pristine nylon substrate	**PEI:rGO**	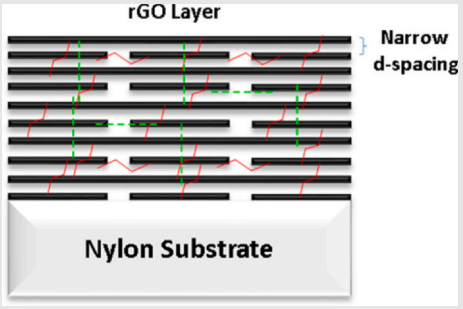
PEI:rGO on a pDA modified nylon substrate	**PEI:rGO/pDA**	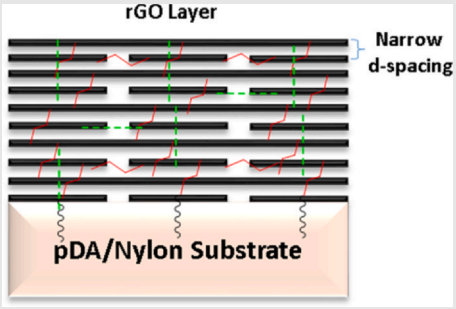
		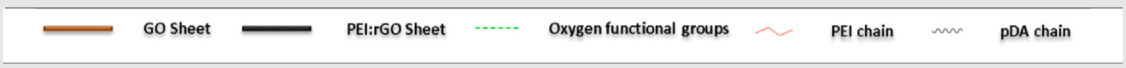

structures of the GO and PEI modified rGO materials were investigated by X-ray photoelectron spectro-scopy (XPS, Versatile UHV XPS System, with a monochromatized Al Kα X-ray source, 1486.6 eV photons and pass energy of 30 eV) and Fourier transform infrared spectroscopy (FT-IR, NICOLET iS10) operated in transmission mode and over wavelength spectrum range between 525 and 4000 cm^{-1} with a resolution of 64 cm^{-1}. Confocal Raman microscope (Renishaw inVia Micro-Raman RE04 System) was used to record Raman spectra of the GO and PEI:rGO materials with a wavelength 532 nm laser and Raman shift range from 500 to 2500 cm^{-1}. Zeta potential analyser (ZP, Malvern Zetasizer Nano ZSP ZEN5600) was also employed to measure the hydrodynamic size diameter (HD) and surface charges of materials through dynamic light scattering (DLS, employing dual-angle measurements 173° and 12.8°). For size analysis, the dispersion samples were initially diluted in DI water by factor of 20 × prior to measurements. X-ray diffraction (XRD, Bruker D2 Phaser diffractometer equipped with a K-Cuα and radiation 1.5406 Å) was employed to determine the d-spacing of GO-based layers with radiation at 40 kV and 30 mA over 2θ range from 5° to 50° and scan rate of 0.25°/min. Water contact angle measurements were performed using an optical tensiometer (SMaRT, KSV CAM 200) to determine surface wettability of membranes based on a sessile drop method at ambient temperatures. GO coatings and microstructure of

pDA coated nylon substrates were confirmed by focused ion beam scanning electron microscopy (FIB-SEM, FEI Helios G4 CX DualBeam) which was operated at 0.1 nA and 2 kV. Field emission scanning electron microscope (FE-SEM, Hitachi SU8230, operated at 2 kV) was employed to analyse surface morphology and microstructures of the GO and PEI:rGO membranes. Prior to SEM analysis, the samples were prepared in small cuts of 1.0 cm × 1.0 cm and coated with carbon. Surface topography analysis of membranes, in terms of surface roughness measurements, was acquired using an atomic force microscopy (AFM, Innova-IRIS Bruker system) run with a non-contact mode and over a scanning area of 1.0 µm × 1.0 µm.

2.4. Evaluation of membrane performance in FO desalination system

The FO performance of the membranes was conducted in a lab-scale FO process, equipped with an in-house built crossflow filtration module, as shown in **scheme (S2)**. The lab-scale membrane cell module was fabricated from acrylic thick sheets for both feed and draw sides with certain specifications, which has an effective membrane area of 6.16 cm^2, as seen in **Fig. (S7)**. The membrane was configured inside the module cell in an FO mode where the active layer was facing the feed solution compartment which was filled with 1 L of 0.1 M NaCl solution. The support substrate was connected to the draw solution compartment which was filled with 1 L of 0.5 M dextrose solution. Prior to the FO experiments, the concentration of the feed and draw solutions were measured and recorded separately to ensure that total dissolved contents in the draw solution side were attributed to changes in the ionic contents of the permeated NaCl salt during the FO operation. This is done by taking the difference between concentration of the DS (which contains NaCl and dextrose) at an interval time and the initial concentration of the dextrose at 0 min. The prepared feed and draw aqueous solutions were circulated counter-currently across the membrane at a room temperature using two gear pumps (Model: 07555–15, Masterflex™, Cole-Parmer™) with a constant flow rate of 200 mL/min (crossflow velocity: 2.3 cm/s). The water flux and salt rejection efficiency were measured after stabilising the fluid flow in the FO system where no bubbles could be observed during the flow circulation. For each salt rejection performance test, the FO system was continuously operated for 6 h. The amount of water permeated across the active area of the membrane was determined by monitoring weight changes of feed solution every 5 min interval time using a digital balance (AND EK-3000i compact, A & D Weighing). The water flux (J_w, **LMH**) was accordingly computed using the following equation (Jang et al., 2020):

$$J_W = \frac{\Delta m}{\rho . \mathbf{A} . \Delta t} \quad (1)$$

Where (Δm) is the mass change of the feed solution using a constant density of DI water (ρ), measured over a time interval (Δt) and permeated across the effective area of the membrane (**A**). Salt retention of membranes was evaluated based on the recorded total dissolved solid (TDS) using a conductivity meter (FiveEasy™ Plus FP30, Mettler Toledo), according to the migrated water quantity and concentration of permeated salt to the draw solution side (C_p) and the initial concentration of the feed solution (C_f). The percentage of salt rejection (**R, %**) was calculated as follows (Jang et al., 2020):

$$\mathbf{R} = \left(\mathbf{1} - \frac{C_p}{C_f}\right) \times \mathbf{100} \quad (2)$$

To assess the internal concentration polarisation (ICP) effects on the membrane performance, the reverse solute flux of permeated NaCl solution from the draw solution side to the feed solution side was determined using the same FO system. In this experiment, 1 L of DI water and 1 L of 0.6 M NaCl aqueous solution were employed as the feed and draw solutions, respectively. The prepared solutions were circulated under the same conditions at ambient temperature and a flow rate of 200 mL/min. The change of concentration of NaCl contents in the feed solution tank was monitored using a conductivity meter over an FO operational time of 3 h. The reverse solute flux (J_s, **gMH**) was calculated using (Fan et al., 2019):

$$J_S = \frac{(C_t m_t) - (C_0 m_0)}{\rho . \mathbf{A} . \Delta t} \quad (3)$$

Where (C_0) and (m_0) are the initial salt concentration and mass of feed solution, respectively, and (C_t) and (m_t) are the corresponding values of salt concentration and feed solution over the FO operation time (Δt). Each experiment was repeated five times, and the average results were reported in this work.

The selectivity factor (*specific flux*, **g/L**) of membranes was determined by dividing the reverse solute flux by the water flux values obtained from the FO evaluation tests as an indication of ICP effects. Thus, the permselectivity of membranes was obtained as follows (Choi et al., 2019):

$$\textbf{Selectivity (specific flux, } J_{SP}) = \frac{J_s}{J_w} \quad (4)$$

2.5. Measurement of transport properties of membranes

The transport properties of membranes, including pure water permeability coefficient **(A)**, salt permeability coefficient **(B)**, structural parameter **(S)** and tortuosity **(τ)** were determined based on the reported protocol (see **Section S5, SI**) (Tiraferri et al., 2013) using a lab-scale pressured filtration RO process, as illustrated in **scheme (S3)**.

3. Results and discussion

3.1. Characterisation of pristine GO and PEI modified rGO laminates

Physicochemical characterisations of the pure GO and PEI doped rGO sheets with optimum concentrations (**Section S2, SI**) were conducted to investigate the chemical functionalisation and structural changes, interlaminar structure, and variation of morphological size, as shown in Fig. (1) and Table (2). The FTIR analysis was employed to determine the functional groups of pristine GO and PEI modified rGO sheets under the transmission mode. As can be observed from Fig. (1.**A**), the un-doped GO has characteristic peaks at the approximate frequency of 3257.8 cm^{-1} which was attributed to the O-H stretching vibration. The low intensity broad peak at 1735.2 cm^{-1} corresponded to the C═O (carbonyl) stretching vibration, whereas the stretching vibration sharp peak at 1625.3 cm^{-1} and 1538.5 cm^{-1} could be

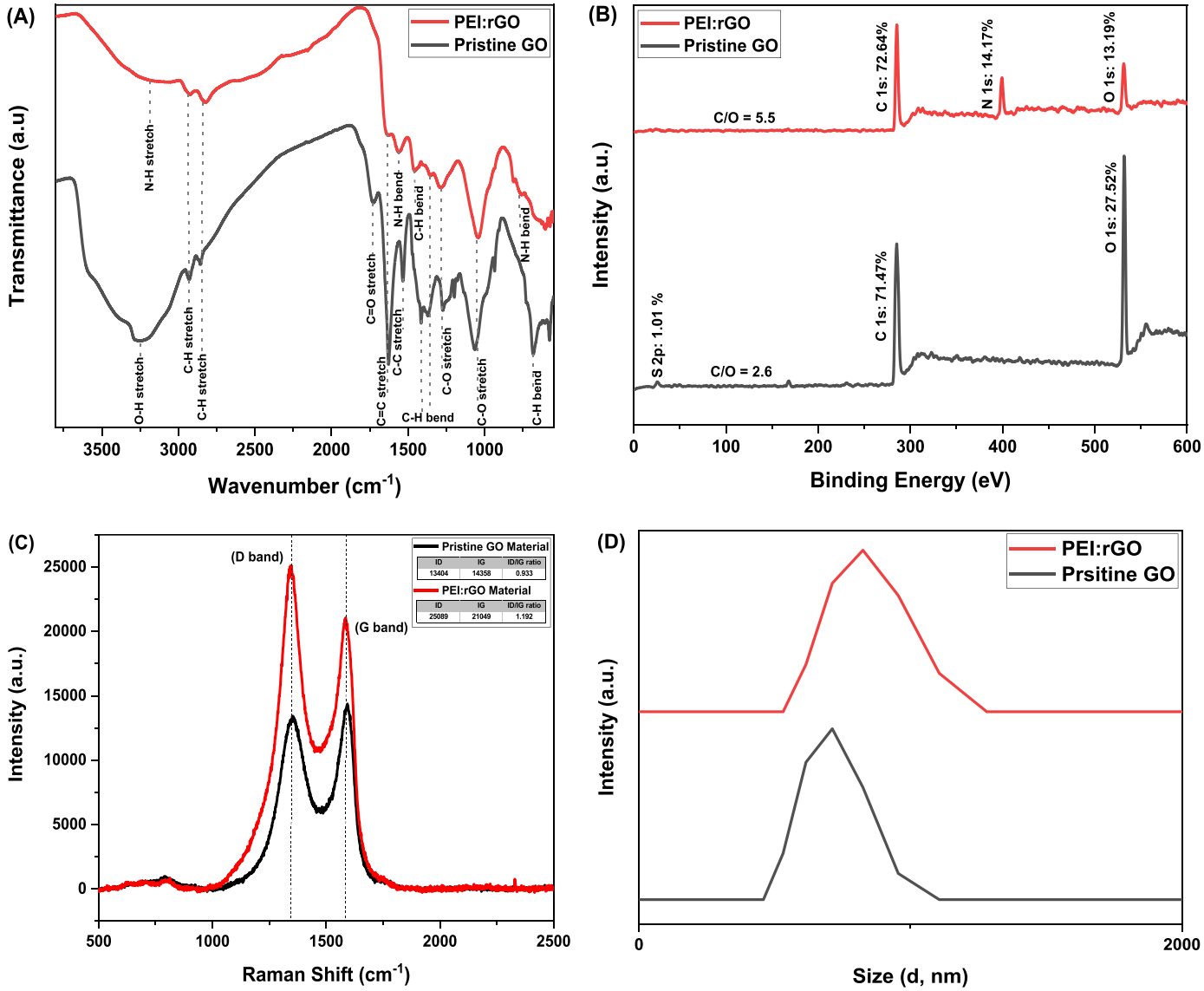

Fig. 1 – Characteristics of freeze-dried pure GO and PEI modified rGO sheets; (A) FT-IR spectra, (B) XPS survey spectra, (C) Raman spectra analysis, (D) DLS particle size distribution profiles.

related to the unoxidized carboxyl groups (C=C bonds), and the C-C bonds, respectively. The FTIR results also showed the presence of alkoxy groups at approximately 1058.3 cm^{-1} (C-O bonds), and epoxy groups at around 1277.1 cm^{-1} which was attributed to the C-O stretching vibration. In addition, the characteristic peaks observed at 685.6 cm^{-1} and 1417.1 cm^{-1}, and 2852.8 cm^{-1} and 2739.6 cm^{-1} were affirmed to the in-plane bending and stretching of C-H, respectively (Lim et al., 2017; Kyzas et al., 2014; Bielawski et al., 2010). After the chemical functionalisation with the branched PEI, the stretching vibration peaks related to the C=O and C-C bonds were disappeared. Moreover, the intensity of the sharp peak of the C=C bonds at 1641.7 cm^{-1} was significantly reduced. This suggests that the total reaction between GO and PEI could be held by the carboxyl and carbonyl functional groups. There are also new peaks observed at a transmittance frequency of 3186.9 cm^{-1} which corresponded to the N-H stretching vibration of primary amine groups, while the broad peaks at 1564.1 cm^{-1} and 768.5 cm^{-1} were attributed to the secondary amine groups of N-H and N-H/C-N bending, respectively. In addition, it was observed that the intensity of peak related to the hydroxyl groups (O-H bonds) was decreased in the PEI:rGO sample. This confirmed the partial reduction of the hydrophilic-containing functional groups as a result of the successful incorporation of the nitrogen-containing amine groups through PEI molecules (Zhou et al., 2015; Wang et al., 2014; Maleki et al., 2017). According to the FTIR analysis, the

Table 2 – Summary comparison for characteristics of pristine GO and PEI doped rGO laminates.

Sample	RAMAN		DLS	SURFACE CHARGE
	I_D/I_G	La (sp^2 cluster size) / nm	Mean particle size / nm	Zeta potential / mV
GO	0.933 ± 0.05	1.27 ± 0.06	935 ± 46.8	- 37.4 ± 1.8
PEI: rGO	1.192 ± 0.06	1.34 ± 0.07	1203 ± 60.2	+ 40 ± 2

interaction and reduction mechanisms between the GO and PEI molecules were expected to be dominated by the two possible chemical structures as follows: (1) carbonyl/carboxyl and (2) epoxy functional groups of GO and amine groups of PEI molecules, as schematically elaborated in **Fig. (S9)**. In the first approach, it was proposed that the carbon atom from carbonyl/carboxyl groups of the GO interacted with the nitrogen atom from the PEI-amino groups through covalent bonding, which vertically formed on the surface of rGO sheets. This could be confirmed by the disappearance of C═O and C═C bonds from the FTIR peaks spectra of the PEI:rGO, and that resulted in the reduction the oxygen-functional groups of GO sheets at temperature of 80 ˚ C (Zhang et al., 2015; Liu et al., 2013; Wang et al., 2013). In the second proposed approach, nucleophilic substitution and condensation reactions were responsible for the formation of covalent bonding between epoxy group of GO and amine group of PEI. In this state, the nitrogen-containing amino group of PEI might attack the epoxy groups of GO, resulting in a proton transfer which could generate water molecules through conversion into hydroxyl groups because of its highly bonding efficiency to the oxygen-containing functional groups. Besides the functionalisation, these reactions would also induce a slight reduction of the GO at high reaction temperatures. The proposed chemical structures between GO sheets and PEI molecules are in a good agreement with the reported literature (Zhou et al., 2015; Liu et al., 2013; Jiang et al., 2015; Sui et al., 2013).

The reactions were further confirmed by XPS spectra analysis, as shown in Fig. (1.**B)** and **Fig. (S10)**. As can be illustrated from the energy survey spectra in Fig. (1.**B)**, the pristine GO only showed two peaks at approximately 285.32 eV and 531.31 eV which were attributed to the carbon (C 1 s) and stronger oxygen (O 1 s), respectively, with the C/O ratio of 2.6. After functionalisation with the PEI, a new peak was observed at 399.32 eV which was corresponded to the presence of the N 1 s. Although, the intensity of the carbon was stronger than that of the oxygen, confirming the successful reduction and modification of GO by nitrogen content through the amino groups of the PEI. For clearer understanding of the reactions (Zhou et al., 2015; Sui et al., 2013; Zhang et al., 2012; Song et al., 2014; Guo et al., 2014), **Fig. (S10)** represents the high-resolution spectrum of C 1 s in both GO and PEI:rGO and N 1 s in the PEI:rGO samples. As can be seen in **Fig. (S10. A)** for the C 1 s of the pristine GO as compared to that in **Fig. (S10. B)** for the PEI:rGO, the pristine GO exhibited three corresponding signals at 286.3 eV, 284.2 eV, and 288.1 eV which were related to the C-O, C-C, and C═O, respectively (Song et al., 2014). For the PEI:rGO framework, new peaks of different intensities were observed at 285.8 eV and 287.7 eV, corresponding to the O-C═O/NH_2 and C-N, respectively (Zhang et al., 2015; Guo et al., 2014). In addition, the peak of the C-O bonding was disappeared, which could be due to the ionic interaction and covalent bonding between the carbonyl/carboxyl functional groups of GO and amine groups of the PEI via the in-situ ''grafting to'' protocol (Liu et al., 2013). As seen in **Fig. (S10. C)** of the N 1 s spectrum of PEI:rGO sheets, the characteristic peaks at 398.9 eV and 400.8 eV confirmed the presence of the abundantly primary (-NH) and weakly secondary (-NH/-CN-) amine groups in the PEI:rGO sample, which agrees with the FTIR results.

Raman spectra analysis also was conducted to confirm the structural changes and chemical reduction and modification of the PEI incorporated GO, as shown in Fig. (1.**C)** and Table (2). The Raman spectra of the pristine GO and PEI doped rGO revealed two characteristic peaks located at 1348.1 cm^{-1} and 1585.7 cm^{-1} which were attributed to the disorder D band of sp^3 defects and crystalline G band of the in-plane sp^2 carbon, respectively. The relative atomic ratio of sp^3 to sp^2 carbons was determined by calculating the relative intensity ratio of D-band and G-band, in terms of I_D/I_G, which is related to the structural properties of the carbon. The addition of PEI into the GO acted as a reductant upon the GO, forming a PEI:rGO structure (Liu et al., 2013; Sui et al., 2013; Zhang et al., 2012; Kuo et al., 2020). This was evident through the study of I_D/I_G values obtained via Raman spectroscopy. Upon addition of the PEI, the I_D/I_G increased from 0.933 to 1.192, leading correspondingly to an increase in the value of La. As GO can be treated as a highly defective material, values of La were determined through direct relationship to the I_D/I_G (*from the Tuinstra Koenig theory* (Tuinstra and Koenig, 1970)), and therefore an increase in I_D/I_G and La values indicated that chemical reduction was successfully conducted and restoration of some graphitic material within the structure of GO was occurred (Liu et al., 2013; Tuinstra and Koenig, 1970; Suk et al., 2010). This could confirm the partial removal of the oxygen-containing functional groups and hence transition of sp^3 carbon into the sp^2 carbon in the PEI:rGO sample. This also indicated the low crystallinity and graphiticity within the structure of the PEI:rGO sheets, which was confirmed by the XRD analysis.

The changes in the hydrodynamic diameter (Lateral size dimension) and surface charge of the pristine and PEI functionalised rGO were confirmed by the DLS data, as presented in Fig. (1.**D)** and Table (2). The DLS results revealed that the incorporation of PEI molecules resulted in increasing the lateral size dimension of the doped rGO sheets of a few hundred nanometers larger than that of the pure GO. This analysis was supported by the TEM and BET data, as illustrated in **Section (S7)**. TEM micrographs showed that the pristine GO and PEI:rGO sheets were in the form of transparent thin sheets (demonstrated by one or two dark lines) with silk-like wrinkled structures and less distortions. This also confirmed the successful chemical functionalisation between the highly orientated GO and PEI crosslinking molecules, which slightly varied the thickness of the formed PEI doped laminates/layers with less structural re-stacking, as confirmed by BET results (Du et al., 2014; Qiao et al., 2015; Nxumalo and Coville, 2010; Ayala et al., 2010). In addition, the surface charge of particles can play a vital role for the stability of dispersible particles and prevent the agglomeration of particles having similar surface charges (Haruna and Wen, 2019). Herein, the formation of highly positive charge on the surface of the PEI:rGO sheets (see **Section S2, SI**) could be beneficial to enhance the salt rejection performance of the prepared membranes (Parsamehr et al., 2019). As a result, it can be summerised that the branched PEI with a controlled low concentration can be an appropriate selection for the fabrication of modified GO-based FO membranes.

The GO and as-synthesised PEI:rGO dispersions were vacuumed filtered to obtain uniformly single GO-based films. The interlaminar structures of the pristine GO and PEI:rGO deposited sheets in dry and wet conditions were examined by XRD patterns through determination of their d-spacing (nano-channels), as seen in Fig. (2.**A)** and Table (3). The d-spacing plays a key role for maintaining the stability, transporting water molecules and selectivity of ionic species which can affect the performance of GO-based membranes

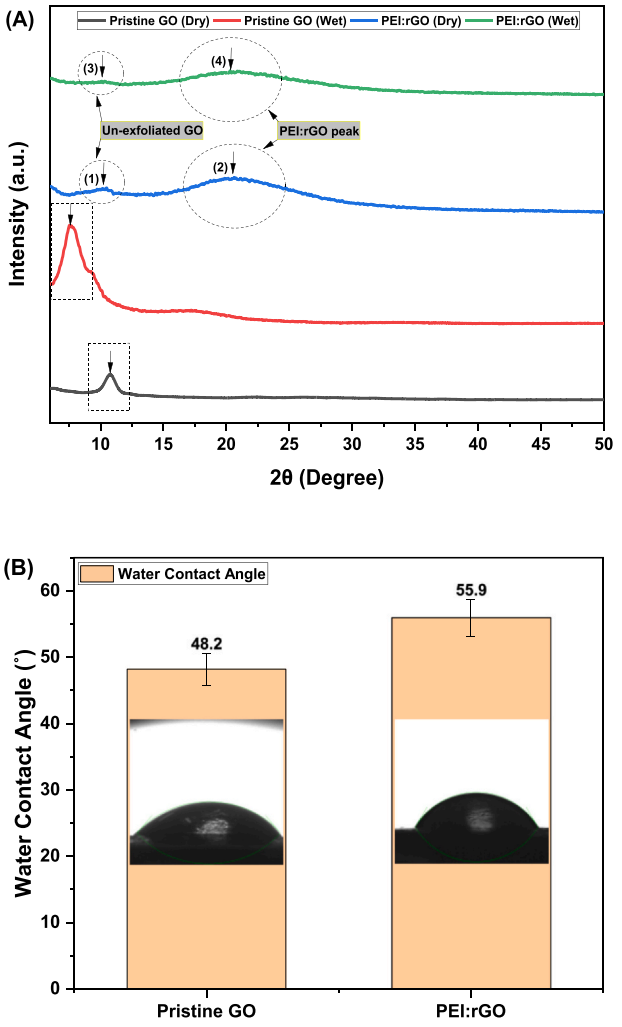

Fig. 2 – *(A)* XRD patterns of the d-spacings in dry and wet conditions and *(B)* water contact angle measurements of the as-fabricated vacuum filtered pristine GO and PEI:rGO laminates.

Table 3 – Interlayer (d-spacing) measurements of GO-based films in dry and wet conditions.

Film	Immersion Time in DI Water (h)	d-spacing (nm)	
		Dry	Wet
Pristine GO	48	0.76 ± 0.038	1.1 ± 0.055
PEI: rGO	48	**(1)** 0.84 ± 0.042 **(2)** 0.47 ± 0.023	**(3)** 0.87 ± 0.043 **(4)** 0.43 ± 0.021

(Song et al., 2019; Lin et al., 2010; Chen et al., 2013). For membranes in dry conditions, upon incorporation of amino groups of PEI into the GO sheets, the XRD peak shifted from $2\theta = 11.78^{\circ}$ to a higher $2\theta = 18.81^{\circ}$ and broadened considerably. These two changes in the diffraction signal suggested that the d-spacing had decreased from 0.76 nm (for GO) to 0.47 nm (for PEI:rGO) and that the crystallite size had decreased (Liu et al., 2013; Yuan et al., 2017), confirming the partial removal of oxygen-containing functional groups, which agrees with our FTIR, XPS and Raman spectra observations. Furthermore, the PEI:rGO laminates exhibited low intensity broad peak occurred at approximately $2\theta = 10.5^{\circ}$ (with a corresponding d = 0.84 nm) which was attributed the presence of un-exfoliated GO into the PEI matrix (Liu et al., 2013). The latter finding could confirm the partial reduction of PEI:rGO sheets and existence of sufficient hydrophilicity for better membrane performance, which was supported by the WCA measurements. For improved salt rejection and stability properties, a smaller d-spacing in the range of 0.7 – 0.3 nm is beneficial, therefore the addition of PEI to bring the modified rGO layers together was preferential for the membrane fabrication in this work (Homaeigohar and Elbahri, 2017). Evidence of PEI cross linking between the GO sheets was seen in the XRD study of both wet and dry PEI:rGO and pristine GO films. After 48 h immersion in water, PEI:rGO laminates showed little to no change in the d-spacing compared to the dry PEI:rGO, contrasting the pristine GO films which showed significant peak shift to a larger d-spacing. In **Fig. (S13)**, it was evident that there was no visual delamination for the PEI:rGO film compared to that of the pristine GO, confirming its excellent stability in wet environments. This provides considerable evidence that the PEI acted as a cross linker between the GO layers, maintaining layer spacing upon the addition of water which acts to swell the GO membrane.

Water contact angle is another crucial parameter which determines the surface wettability of membranes and their filtration performance (Yang et al., 2018). As shown in Fig. (2.**B**), the contact angle of the PEI:rGO layer was slightly higher than that of the pristine GO, due to the partial chemical reduction of the oxygen-containing functional groups of GO upon the addition of amino groups from PEI molecules and hence reducing graphitic materials on the surface of PEI:rGO film, which is in a good agreement with our FTIR, XPS, Raman and XRD analysis. The increase in the contact angle measurement implies that the PEI:rGO layer obtained slightly lower surface wettability than that of the pristine GO. Despite the lower hydrophilicity of the PEI:rGO laminates, it can be elucidated that the amount of oxygen and nitrogen functional groups recovered by the un-exfoliated GO and incorporation of PEI, respectively, could be sufficient to keep the crosslinked PEI:rGO film in the range of the hydrophilic surfaces, as reported in the literature (Lim et al., 2017).

3.2. *Morphological properties of GO-based laminated membranes*

Optical morphologies of the membranes are represented by the digital images shown in **Fig. (S14)**. Surface morphology and topography, and cross-section of the GO-based pDA membranes are presented in Fig. (3), **Fig. (S15)**, **Fig. (S17)**, and **Fig. (S18)**. Fig. 3 **(A-i)** and **(A-ii)** show the whole FIB-SEM cross-section images of the GO/pDA and PEI:rGO/pDA membranes, respectively. In these images, it can be seen that the pDA coating was well-packed and tightly developed with the nylon support structures. It should be noted that the denser appearance of the cross-sectional FIB-SEM images for pDA coating in Fig. (3-**A)** is an artefact from the FIB preparation of the sample that lead to some smearing out of the pDA coating around the nylon fibres, resulting in a denser appearance. In addition, it was clearly observed that GO and PEI:rGO films were tightly entwined and stacked with the pDA layer via non-covalent bonding which resulted from the interfacial adhesion process (Zhang et al., 2015; Lv et al., 2018). Interestingly, the pDA coating with the optimum concentration of 0.5 mg/mL (and coating time of 1.5 h) did not show any sign of pDA aggregates, or even cause any obvious pore blockages on surface of the nylon substrate, as shown in Fig. S19 **(B-i)** similarly to the surface of pristine nylon

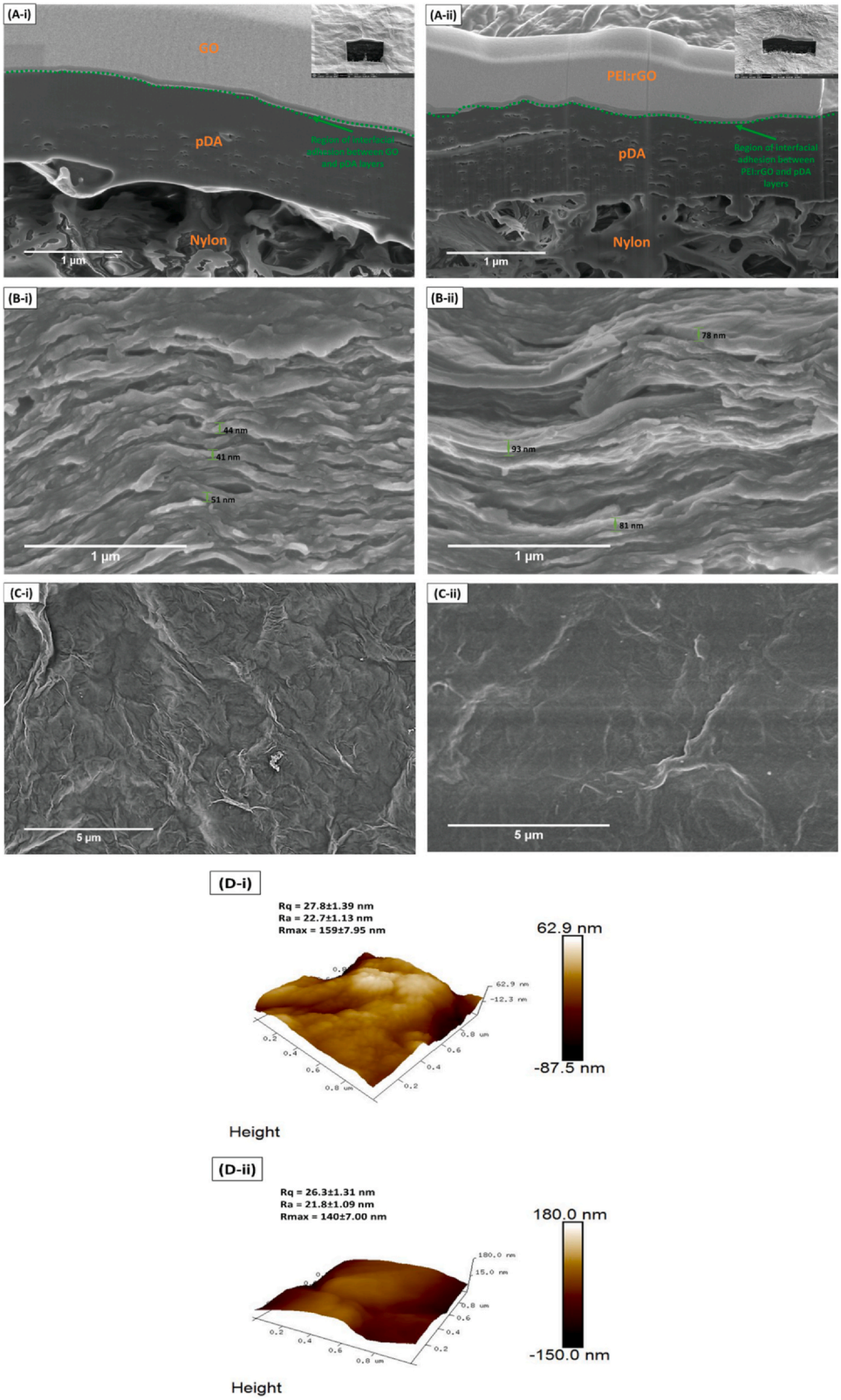

Fig. 3 – Morphological characteristics; (A) FIB-SEM cross-section images (inset FIB-SEM images show cropped cross-sectional area of membranes), (B) SEM cross-section images, (C) SEM surface images, and (D) AFM topography analysis of the pristine GO (denoted by (i)) and PEI:rGO laminates deposited on the pDA coated nylon subsrates (denoted by (ii)).

substrate in Fig. S19 **(A-i)**. This could significantly contribute to enhance the desalination performance as a result of increasing water molecule adsorption sites after passing through the GO-based active layers (Li et al., 2014). Fig. 3 **(B-i)** and **(B-ii)** reveals FE-SEM images of the GO and PEI:rGO laminates successfully assembled into highly ordered films on the top of the interfacial layer of pDA via a vacuum filtration method, respectively. In addition, Fig. S22 **(A)** and **(B)** show the thicknesses of the GO and PEI:rGO layers in nano-meter scales which were tested during the FO performance process. As can be indicated that the PEI:rGO exhibited well-laminated and continuous structure which was parallel to the

surface of the filter membrane, compared to that of the delaminated structure of GO sheets. During chemical functionalisation, it should be noted that the PEI molecules would decorate on the surface of the GO sheets and hence form continuous phase structure, creating a robust PEI:rGO film with excellent mechanical properties (Liu et al., 2013; Yuan et al., 2017). This was clearly shown in Fig. 3 **(B-ii)** and Fig. S22 **(B-i, ii, and iii)**. As also can be observed in Fig. 3 **(B-ii)**, the layered PEI:rGO film demonstrated less pore distribution (i.e., nanochannels) between PEI:rGO sheets compared to the layered GO film Fig. 3 **(B-i)**. This was attributed to partial chemical reduction of the oxygen-containing functional groups of the GO after crosslinking with PEI molecular chain, resulting in more compact structure and narrower d-spacing between PEI:rGO layers. Fig. 3 **(C-i)** and **(C-ii)** illustrate the surface morphology of the GO and PEI:rGO films deposited on the top of pDA-coated nylon substrate, respectively. Here, as can be observed was that the GO/pDA membrane exhibited a typically wrinkled morphology. After crosslinking process with the PEI, the PEI:rGO/pDA membrane had less wrinkles on the surface. This can propose that the incorporation of PEI into the GO and accordingly reduction of the graphitic layers could bring a significant impact on the formation of wrinkles (Yan et al., 2017b; Zhang et al., 2015; Parsamehr et al., 2019; Dikin et al., 2007). However, the pDA coating on the nylon filter also plays a vital role in the augment of surface morphologies. To verify this effect, the GO and PEI:rGO films which were deposited on the pristine nylon substrates, showed more wrinkled morphology than that of the GO-based films assembled on the surface of the pDA coated nylon membranes, as observed in Fig. S17. This was attributed to increasing the surface roughness of the commercial nylon fibers, which is supported by the AFM analysis (Kim et al., 2017). AFM topography analysis was also employed to further evaluate surface morphologies of GO/pDA and PEI:rGO/pDA membranes, as shown in Fig. 3 **(D-i)** and **(D-ii)**, respectively. Here, it was clear that the crosslinking of GO sheets with PEI resulted in a slight reduction of the surface roughness measurements. As previously mentioned, this was due to the partial removal of the oxygen-containing functional groups and defects on the surface of GO layer. Again, the pDA coating on the surface of nylon membrane played a vital role in decreasing the surface roughness of layered GO and PEI:rGO films and covering the defects on the surface of the pristine nylon fibers. As shown in **Table. (S4)**, the GO and PEI:rGO layers assembled on the pristine nylon substrates showed relatively higher surface roughness values than those deposited on the pDA coated nylon filters. The AFM observations are in a good agreement with our SEM analysis.

3.3. *Desalination performance of membranes in an FO process*

The FO membrane desalination performance, in terms of water flux and salt rejection, as a function of the GO loading for GO/pDA, PEI:rGO, and PEI:rGO/pDA membranes are shown in **Fig. (S23, Section 8, SI)** and corresponding values are summarised in **Table. (S6)**. As can be observed, the water flux and salt rejection of membranes increased and decreased, respectively, with decreasing the GO loading and thickness of GO-based films. This finding is consistent with the reported literature (Parsamehr et al., 2019). Generally, the pristine GO film deposited on the top of pDA/nylon substrate, as a reference membrane, exhibited higher water permeability, but lower salt rejection, than PEI:rGO and PEI:rGO/pDA membranes. It can also be seen that PEI:rGO membrane indicated a lower water permeation than that of the PEI:rGO/pDA membrane but with close salt retention values. The reasons for this behaviour are discussed in **Section (3.5)**. Smaller thickness generally results in better water flux but will lead to lower structure stability over prolonged period of usage. Based on the balance between the membrane performance and structural stability, the GO and PEI:rGO films fabricated by 0.167 and 0.329 mg/cm^2, respectively, were selected as optimised loadings for the GO-based membranes with their associated water flux and salt rejection throughout the study, as shown in **Table. (S6)**.

Fig. (4) presents a comparison of FO water permeation and salt rejection performances between the GO-based membranes and the commercial CTA-FO membrane. The structure of the membranes plays a crucial role in influencing their FO performances, as reported in the literature (Song et al., 2019; Padmavathy et al., 2019). Remarkably, all GO-based layered membranes exhibited higher water permeation rates than the

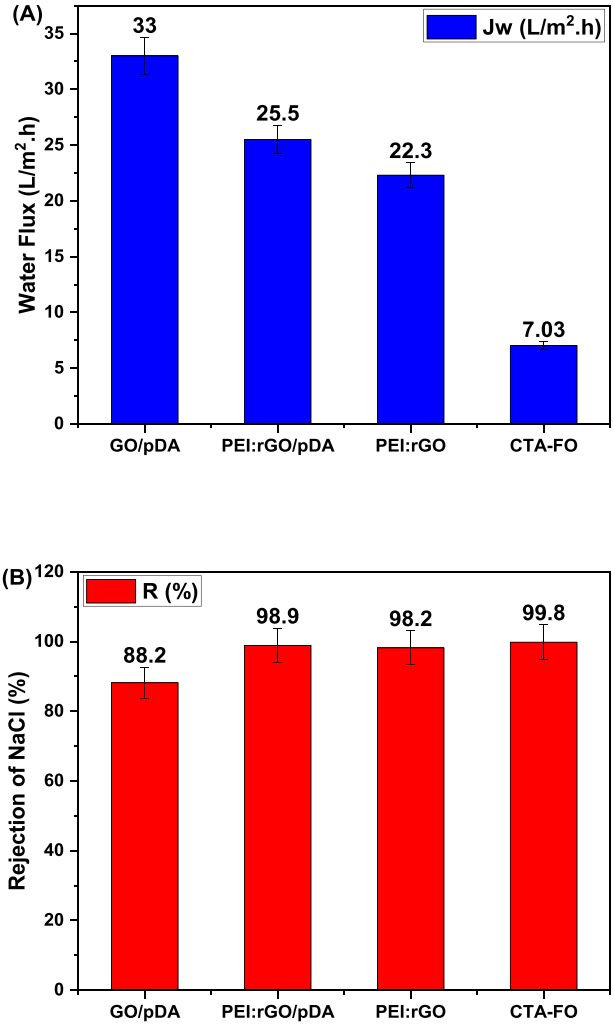

Fig. 4 – (A) water permeation and (B) salt rejection performance of GO-based membranes with the optimum loading of GO-based material, compared to the commercial CTA-FO membrane. (Experimental conditions: 0.1 M NaCl and 0.5 M dextrose were employed as feed and draw solutions, respectively, in FO mode at a crossflow rate of 200 mL/min).

commercial CTA-FO membrane, but their salt rejection efficiencies were slightly lower, which is consistent with previously reported researches (Sahebi et al., 2017; Liu et al., 2015). The GO/pDA membrane demonstrated the highest water flux performance but suffered from significantly lower salt rejection than both the CTA-FO and PEI:rGO-based membranes. This difference can be attributed to the increased d-spacing (nanochannel size) due to the severe swelling of laminar GO sheets in wet conditions, as confirmed by XRD analysis in Fig. (2.**A**). This could allow more Na^+ and Cl^- ions to easily migrate and diffuse through the active layer of the GO. Conversely, the PEI:rGO-based membranes showed the second highest water permeability, comparable to the commercial CTA-FO membrane, and exhibited similar salt rejection rates. This behavior was a result of the reduction in d-spacing caused by cross-linking GO with PEI, slightly increasing the hydrophobicity of non-oxidized regions in the nano-channels and on the surface of PEI:rGO films. Despite the chemical reduction of GO by PEI, the introduction of nitrogen-containing groups in PEI rendered the membrane more hydrophilic due to interactions with water through H-bonding (Lim et al., 2017). The addition of pDA to the nylon support layer (PEI:rGO/pDA membrane) also contributed to increased hydrophilicity, as evidenced by the lower WCA of pDA-coated nylon filter (Fig. S19). This enhancement in hydrophilicity improved water flux and facilitated water entry after crossing the PEI:rGO films to the permeate side. Additionally, incorporating both PEI and pDA had an effect on the membrane charge, based on the Donnan exclusion theory, leading to increased salt rejection of NaCl. To assess the anti-fouling ability (*resistance to foulants deposition*) of the GO-based membranes, EDX elemental mapping analysis was conducted after the FO desalination tests. The results showed that the PEI:rGO/pDA membrane exhibited the least NaCl deposition, followed by PEI:rGO and GO/pDA membranes (Fig. S24). The interfacial layer of pDA played a crucial role in mitigating NaCl permeation and adhesion, thereby increasing the anti-fouling ability through its hydrophilic surface, which is consistent with our FO desalination results.

3.4. *Investigation of ICP effects on performance of membranes*

The study also considered the impact of asymmetric structure of optimal membranes, including reverse solute flux (RSF), water flux, and specific salt flux in an FO process. Measurements were carried out using DI water and 0.6 M NaCl as feed and draw solutions, respectively. Fig. (5) presents the results of GO-based membranes, compared to a commercially available CTA-FO membrane under the same FO conditions. Fig. (5.**A**) shows that the PEI:rGO/pDA membrane achieved the highest average water flux (18.8 ± 0.9 LMH), followed by PEI:rGO (13.5 ± 0.6 LMH), GO/pDA (9.9 ± 0.5 LMH), and CTA-FO (2.6 ± 0.2 LMH) membranes. The presence of support layers in the FO system impacts the osmotic pressure gradient, affecting water flux and increasing reverse solute flux (Huang et al., 2013b). However, the selection of a highly porous nylon support filter and further pDA modification reduced water permeation hindrance and osmotic pressure difference, leading to higher water flux for the PEI:rGO/pDA membrane. The incorporation of PEI into GO laminates also created low-friction hydrophobic nano-channels (Liu et al., 2015), while the pDA coating on the nylon substrate hindered reverse NaCl flux, resulting in the lowest reverse solute flux for the PEI:rGO/pDA membrane (Fig. 5.**B**). Nevertheless, the reduction in water

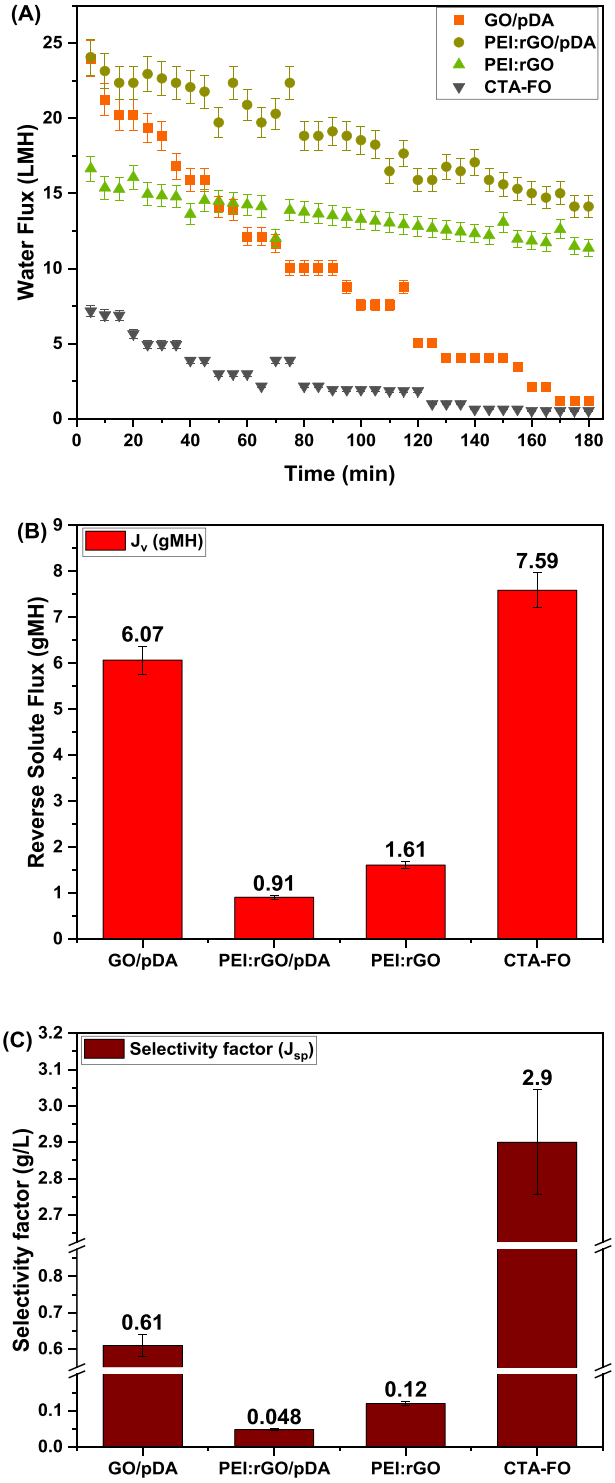

Fig. 5 – (*A*) Water flux, (*B*) reverse solute flux, and (*C*) specific solute flux of commercial CTA-FO and GO-based membranes tested in an FO system at a crossflow rate of 200 mL/min and ambient temperature using DI water and 0.6 M NaCl as feed and draw solutions, respectively.

flux observed in the PEI:rGO/pDA membrane over an FO operational time, as compared to the PEI:rGO membrane, can likely be attributed to the pDA coating during fabrication, the same phenomenon also observed in the GO/pDA membrane. This coating process may promote the accumulation of pDA material within the pores of the modified substrate (Yang et al., 2017; Zhang et al., 2015). Despite the slight decrease in water flux in the PEI:rGO/pDA membrane relative to the PEI:rGO membrane, this is offset by a significant reduction in

Table 4 – Intrinsic water/ion transport properties of the membranes tested in RO pressurised filtration process; water permeability (A), salt permeability (B), structural parameter (S), porosity (ε), thickness (t) and tortuosity (τ).

Membrane	A (LMH/bar)	B (LMH)	A/B (1/bar)	S (μm)	ε (%)	t (μm)	τ
GO/pDA	2.19 ± 0.11	1.91 ± 0.09	1.15 ± 0.06	275 ± 13.7	75.87 ± 3.79	82.09 ± 4.05	2.54 ± 0.13
PEI: rGO/pDA	1.98 ± 0.09	0.17 ± 0.01	11.5 ± 0.57	67 ± 3.35	75.58 ± 3.78	82.24 ± 4.08	0.61 ± 0.03
PEI:rGO	1.87 ± 0.09	0.22 ± 0.01	8.3 ± 0.41	71 ± 3.25	73.38 ± 3.67	80.24 ± 4.01	0.65 ± 0.03
CTA-FO	1.69 ± 0.08	0.38 ± 0.02	4.43 ± 0.22	476 ± 23.8	64.45 ± 3.22	50 ± 2.50	6.14 ± 0.31

reverse salt flux and an improvement in both mechanical and chemical stability (see Section 3.6). This ensures that the water flux of the PEI:rGO/pDA membrane remains at an acceptable level. To better understand the RSF phenomenon, NaCl ion permeation from the draw side to the feed side across membranes was investigated (Fig. S25). The PEI:rGO/pDA membrane had the lowest ion permeation rate, compared to the GO, CTA-FO, GO/pDA, and PEI:rGO membranes. This reduction was attributed to ion size exclusion and surface charge modification (see Section 3.5) (Homaeigohar and Elbahri, 2017). The additional decrease in ion permeability for the PEI:rGO/pDA membrane was due to the incorporation of the pDA coating on the nylon filter, which further retarded reverse salts, reducing the ICP effects. Fig. (5.C) displays the selectivity factor (J_s/J_w) for each membrane, which represents the lost quantity of reverse draw solute per unit of water (Deka et al., 2021). The PEI:rGO/pDA membrane exhibited the lowest specific salt flux, confirming its superior FO performance. These findings are aligned with the results for intrinsic membrane properties presented in Table (4).

Table (4) indicates the obtained results for transport separation properties of all membranes. As can be observed, the structural parameter value plays a vital role to determining the effects of ICP within the porous structure of substrate, the low structural parameter (S) and tortuosity (τ) values propose that the ICP is weakly affecting the support layer of composite membranes. Herein, as the two PEI:rGO membranes have the same structure for the selective layers, the slight difference in the water flux was due to the incorporation of the pDA coating onto the nylon substrate. This can confirm that the PEI:rGO/pDA membrane showed the best salt selectivity value, followed by the PEI:rGO, GO/pDA and CTA-FO membranes. The latter findings were consistent with the obtained results from FO desalination and ICP evaluation systems.

3.5. *Conceptual mechanism for PEI:rGO/pDA membrane*

The mechanism responsible for the remarkable improvement in water flux, salt retention, and transport properties across the PEI:rGO/pDA membrane is visually illustrated in Fig. (6). This enhanced performance can be attributed to three key factors. Firstly, comparing the hydrated diameters of Na^+ and Cl^- ions (0.72 nm and 0.66 nm, respectively (Xu et al., 2016); Cohen-Tanugi and Grossman, 2015), to the d-spacing of the PEI:rGO laminates (Fig. 2.A and Table 3), one could assume that the PEI:rGO film would serve as a barrier against the permeation of salt ions in both directions due to size exclusion effects within the nanochannels formed between stacked PEI:rGO sheets. Consequently, this leads to an enhanced salt rejection efficiency and significantly reduced reverse solute flux and internal concentration polarisation (ICP) when compared to the

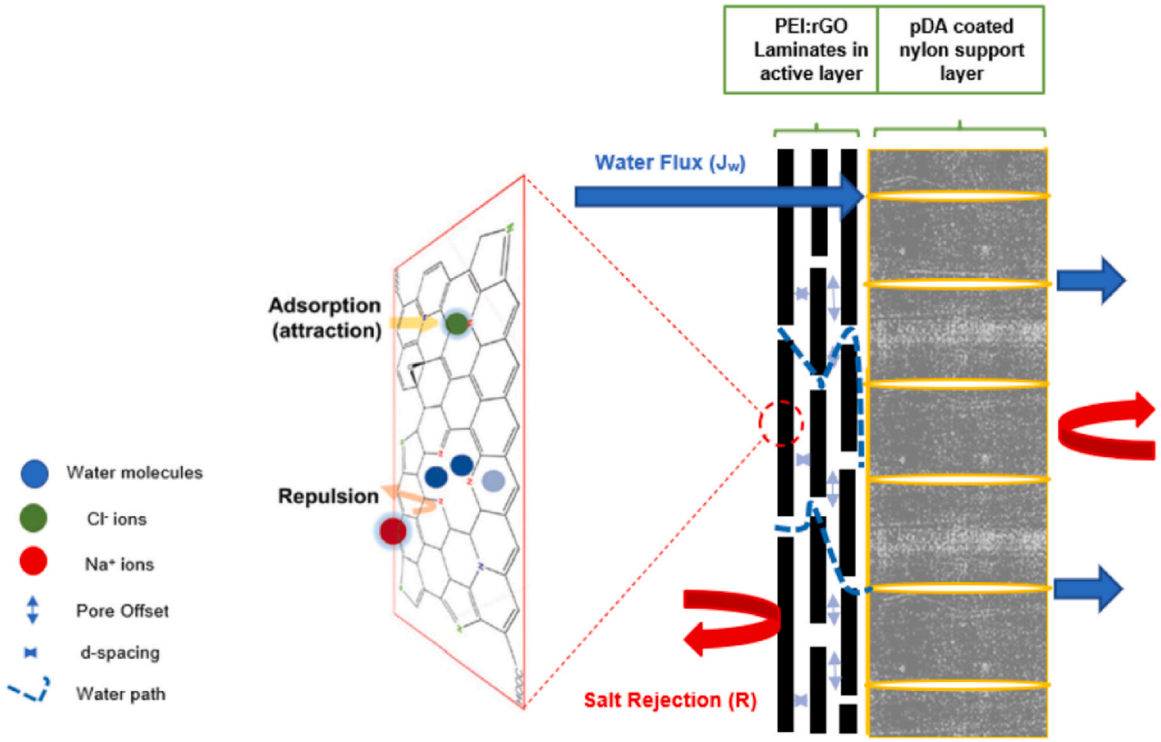

Fig. 6 – Schematic of water/ions desalination/salt retention mechanism across the robust PEI: rGO/pDA membrane.

(A)	(Exposure Time in 0.6 M NaCl)					
Membrane	Day 1	Day 10	Day 20	Day 30	Day 40	Day 60
GO	4	3	2	1	1	0
GO/pDA	5	5	4	3	1	0
PEI: rGO	5	4	4	2	1	0
PEI: rGO/pDA	5	5	5	5	5	4

(B)	(Exposure Time in 1,000 ppm NaClO)			
Membrane	3 min	30 min	3 h	27 h
GO	4	3	0	0
GO/pDA	5	4	4	4
PEI: rGO	5	5	5	1
PEI: rGO/pDA	5	5	5	5

Excellent (Score: 5) Good (Score: 4) Fair (Score: 3-2) Poor (Score: 1-0)

Fig. 7 – Evaluation of dimensional stability and durability of GO-based membranes and nylon substrates (*based on an industrial score rating*), exposed to an ionic (*A*) 0.6 M NaCl solution, and (*B*) NaClO chlorine-containing solution of various concentrations over different periods.

GO/pDA reference membrane. Moreover, the balanced osmotic pressure across the PEI:rGO film is well-maintained, which aids in effective water transport near the membrane surface. Secondly, the incorporation of hydrophilic properties on the membrane surface, achieved through the chemical cross-linking of GO with PEI and the addition of pDA onto the nylon support filter, plays a pivotal role. Although the chemical reduction of GO with PEI may slightly hinder forward water transport, the introduction of nitrogen-containing groups in PEI ensures that the membrane remains in the hydrophilic range, as supported by water contact angle measurements. The presence of pDA further enhances the hydrophilicity, providing aromatic alcohol groups that create polarity and less roughness on the nylon filter surface, allowing better interaction with water and reducing ICP effects. However, the impact of pDA coating on the overall porosity and pore connections between PEI:rGO laminates and the pDA-coated nylon filter, in relation to the water permeation, requires further investigation. Despite this, the synergetic effects of incorporating PEI and pDA, both capable of interacting with water through hydrogen bonding, contribute to acceptable water permeation and superior salt rejection in the PEI:rGO/pDA membrane (Lim et al., 2017; Yuan et al., 2017; Roy and Kim, 2019; Ding et al., 2016; Li et al., 2011; Wang et al., 2015). Lastly, the membrane surface charge significantly influences NaCl salt rejection via the Donnan exclusion effect. The positively charged PEI:rGO can generate electrostatic repulsion against Na^+ cations during FO salt rejection tests. In addition, the presence of negatively charged and un-exfoliated GO on the surface and within the microstructure of the active layer can also repel some of Cl^- ions but some could be adsorbed due to the higher diffusivity of Cl^- anions compared to the Na^+ cations. On the other hand, the negatively charged pDA-coated nylon support layer maintains enough electrostatic repulsion against anions (e.g., Cl^- ions during FO-ICP evaluation). Although the pDA-coated nylon membrane possesses a weaker negative surface charge, it still contributes to a certain extent in enhancing salt rejection (Zhang et al., 2015; Parsamehr et al., 2019). Additionally, counter-ions are likely rejected through an adsorption effect on the membrane surface or within its microstructure, but the exact reasons behind this effect require further exploration. In summary, the synergistic combination of these key factors results in the exceptional FO performance of the PEI:rGO/pDA membrane, making it a promising candidate for advanced desalination applications.

3.6. *Evaluation of membranes structural stability*

As recently reported in the literature, there is still on-going challenge with the physical and chemical stability of the laminated GO-based membranes in FO process (Wu et al., 2020). Typically, the industrial application of FO for water

Membrane	(Structural durability in ultrasonication)					
	0 min	1 min	3 min	10 min	30 min	≥ 60 min
GO	4	4	2	0	0	0
GO/pDA	5	4	2	1	0	0
PEI: rGO	5	5	4	3	2	1
PEI: rGO/pDA	5	5	5	5	5	5

Stable (Score: 5) Disassembled (Score: 4) Deformed (Score: 3-2) Critically damaged (Score: 1-0)

Fig. 8 – Assessment of structural integrity and durability (*based on an industrial score rating*) of modified GO membranes exposed to ultrasonication in water.

treatment and purification involves protocols, including chemical washing and hydraulic backwashing, which are important for the recovery of the membrane performance. Therefore, it was necessary to evaluate our resultant PEI:rGO/pDA membrane and compared to the other fabricated GO-based membranes, in chemical and harsh conditions.

The ionic and chlorine tolerance of the as-prepared GO-based membranes were assessed as a function of time using aqueous solutions of sodium chloride (0.6 M) and sodium hypochlorite (at different concentrations of 1000, 10,000 and 30,000 ppm). The obtained evaluation analysis and associated digital images of membranes exposure are presented in Fig. (7) and **(S26 – S28)**. Here, the chemical resistance evaluation was conducted similar to the assessment procedures followed in water treatment industrial systems. As shown in Fig. (7.**A)** (*Supported by* **Fig. (S26)**), the PEI:rGO/pDA membrane possessed an outstanding structural integrity when exposed to NaCl solution for 60 days, compared to that for other GO-based membranes. Similarly, after 27 h exposure to NaClO solution of three different concentrations, the resultant PEI:rGO/pDA membrane showed negligible change in terms of the dimensional stability, better than that of the other fabricated GO membranes, as depicted in Fig. (7.**B)** (*Supported by* Fig. S27 and S28)). Furthermore, it should be noted that only low concentrations of sodium hypochlorite are used during chemical washing of membranes in the industrial processes (Kim et al., 2017; Li et al., 2019b). Accordingly, the resultant PEI:rGO/pDA membrane implied a high confidence in the chlorine resistance. As explained above, the improved structural integrity and durability of the resultant PEI:rGO/pDA membrane, in comparison to other GO membranes, was attributed firstly to cross-linking of GO and reduction of its d-spacing by introduction of PEI-based amino groups which prevented the separation and swelling between the neighbouring PEI:rGO sheets in wet ionic and chlorine environments. Moreover, the pDA coating onto the nylon filter essentially provided more anchoring sites to tightly hold the stacked PEI:rGO sheets through forming numerous bonds that maintained its initial structure. These observations further demonstrated the long-term and enhanced stability of the PEI:rGO/pDA membrane during chemical washing procedures.

The mechanical stability of the GO-based membranes was evaluated and compared after the FO desalination test. The active layer of the pristine GO membrane collapsed after 5 h in the FO lab process, and hence was excluded from the dimensional stability testing. The other tested GO membranes were vigorously exposed to hydraulic backwashing by counter-currently passing DI water on both sides of the membranes at 1236 mL/min for 15 min. As can be observed in Fig. S29 **(A-i – C-i)**, photographs of membranes showed no visual delamination for the tested membranes. However, corresponding SEM images, shown in Fig. S29 **(A-ii – C-ii)**, revealed that the PEI:rGO/pDA membrane stood out as the most stable membrane among the other tested membranes, and its structure remained unchanged. Whereas GO/pDA and PEI:rGO membranes showed some fractures on the surface of membranes. This could confirm that the combination between the unique chemical properties of PEI:rGO sheets and pDA molecules were well matched to improve the stability of PEI:rGO/pDA membrane alone in harsh conditions. Interestingly, the resultant membrane exhibited excellent a long-term dimensional stability when exposed to ultrasonication in DI water for approximately 100 min, compared to other GO-based membranes as shown in Fig. (8) (*Supported by* **Fig. (S30)**).

Table 5 – Performance comparison of water permeability, salt rejection and dimensional stability of the PEI/pDA modified GO-based membranes prepared for different desalination processes reported in this work and other studies in literature.

Membrane	Water Flux (LMH)	NaCl Rejection (%)	Feed Concentration (M)	Desalination Process	Stability	Thickness of GO layer (nm)	GO Material Loading mg/cm^2	Ref.
GO/pDA	33	88.2	0.1	FO	–	~98.34	0.167	**This Work**
PEI: rGO	22.3	98.2	0.1	FO	Chemically	~240.7	0.329	**This work**
PEI: rGO/pDA	25.5	98.9	0.1	FO	Mechanically/ chemically	~240.7	0.329	**This Work**
NHS/EDC-GO-PEI	7	55	0.06	RO/NF	Mechanically	1500	0.4	(Parsamehr et al., 2019)
GO-EDA-HPEI	5.5	58	0.03	NF	Mechanically	100	0.083	(Zhang et al., 2015)
GO-PEI	4.2	38	0.03	RO	–	17,100	–	(Jia and Wang, 2015)
TA-GO-PEI	15	64	0.03	RO/NF	Chemically	1300	–	(Lim et al., 2017)
pDA-rGO	36.6	92	0.1	FO	–	170.4	–	(Yang et al., 2017)

As presented in Table (5), the FO desalination performance and structural stability of the PEI:rGO/pDA membrane is comparable to other PEI and pDA modified GO-based laminar membranes reported in the literature (Yang et al., 2017; Zhang et al., 2015; Lim et al., 2017; Parsamehr et al., 2019; Jia and Wang, 2015). Besides its excellent mechanical and chemical stability, our resultant membranes showed an acceptable FO performance which can provide good balance with its dimensional stability.

4. Conclusion

In this work, the reduction and hydrophilic modification of GO-based membranes were successfully achieved by in situ grafting of PEI into the laminated GO sheets and coating of pDA onto the nylon substrate, respectively, at noticeably low chemical concentrations. The protocol of combining chemical functionality of N-amine groups of PEI and pDA was synergistically effective for the fabrication of robust rGO-composite membranes with good hydrophilicity. The cross-linking of GO sheets with PEI led to controllable reduction of oxygen-containing functional groups and narrowing d-spacing between GO laminates, and hence creating hydrophilic, defect-free, and less rigid rGO membrane surface. Moreover, the modification of the nylon substrate with the pDA effectively contributed to reducing ICP effects and tortuosity of the resultant PEI:rGO/pDA membrane. The latter findings were resulted in improving the FO desalination performance and lowering ICP effects, compared to the GO-based and commercial CTA-FO membranes. Besides, the entwined structure of the PEI:rGO/pDA membrane, along with induced surface electrostatic charges, experimentally exhibited an average water flux of 25.5 L/m^2.h, salt rejection of 98.9% and reverse solute flux of 0.91 gMH in the FO process, as compared to the other tested membranes. In addition, the PEI:rGO/pDA membrane feasibly maintained an excellent structural integrity, chemically and mechanically, during long testing periods in ionic and chlorine solutions and under harsh conditions, respectively. Therefore, it is proposed that the obtained findings can provide a promising research insight for scaling-up membrane materials, and cooperatively provide a breakthrough for overcoming the ongoing trade-off between the desalination performance and long-term stability in FO application. Besides, our future study is focused on the investigation of the electro-conductivity potential of as-synthesis PEI:rGO nano-composites for improving water permeability and FO membrane performance with the aid of electrical field.

Declaration of Competing Interest

The authors declare that they have no known competing financial interests or personal relationships that could have appeared to influence the work reported in this paper.

Acknowledgements

The authors would like to acknowledge the financial support from the Ministry of Higher Education and Scientific Research – State of Libya. We also acknowledge the technical support provided by Dr Ben Douglas from school of chemical and process engineering, Mr Stuart Micklethwaite and Dr Zabeada Aslam from Leeds Electron microscopy and spectroscopy centre (LEMAS), and Dr Christopher Pask from school of chemistry at the University of Leeds.The support from the Henry Royce Institute (EPSRC grants: EP/P022464/1, EP/R00661X/1), which funded the VXSF Facilities (https://engineering.leeds.ac.uk/vxsf) within the Bragg Centre for Materials Research at Leeds is also acknowledged.

Appendix A. Supporting information

Supplementary data associated with this article can be found in the online version at doi:10.1016/j.cherd.2023.10.022.

References

Abraham, J., et al., 2017. Tunable sieving of ions using graphene oxide membranes. Nat. Nanotechnol. 12 (6), 546.
Aghehrochaboki, R., et al., 2019. Polyethyleneimine functionalized graphene oxide/methyldiethanolamine nanofluid: Preparation, characterization, and investigation of CO_2 absorption. J. Environ. Chem. Eng. 7 (5), 103285.
Akther, N., et al., 2015. Recent advancements in forward osmosis desalination: a review. Chem. Eng. J. 281, 502–522.
Ayala, P., et al., 2010. The doping of carbon nanotubes with nitrogen and their potential applications. Carbon 48 (3), 575–586.
Bielawski, C., et al., 2010. The chemistry of grapheme oxide. Chem. Soc. Rev. 39 (1), 228–240.
Castelletto, S., Boretti, A., 2021. Advantages, limitations, and future suggestions in studying graphene-based desalination membranes. RSC Adv. 11 (14), 7981–8002.
Cath, T.Y., Childress, A.E., Elimelech, M., 2006. Forward osmosis: principles, applications, and recent developments. J. Membr. Sci. 281 (1–2), 70–87.
Chen, J.-T., et al., 2013. Tuning nanostructure of graphene oxide/polyelectrolyte LbL assemblies by controlling pH of GO suspension to fabricate transparent and super gas barrier films. Nanoscale 5 (19), 9081–9088.
Choi, H.-g, et al., 2019. Thin-film composite membranes comprising ultrathin hydrophilic polydopamine interlayer with graphene oxide for forward osmosis. Desalination 449, 41–49.
Cohen-Tanugi, D., Grossman, J.C., 2015. Nanoporous graphene as a reverse osmosis membrane: recent insights from theory and simulation. Desalination 366, 59–70.
Deka, P., et al., 2021. Performance evaluation of reduced graphene oxide membrane doped with polystyrene sulfonic acid for forward osmosis process. Sustain. Energy Technol. Assess. 44, 101093.
Dikin, D.A., et al., 2007. Preparation and characterization of graphene oxide paper. Nature 448 (7152), 457–460.
Ding, Y., Floren, M., Tan, W., 2016. Mussel-inspired polydopamine for bio-surface functionalization. Biosurf. Biotribol. 2 (4), 121–136.
Du, M., et al., 2014. Synthesis of nitrogen-doped reduced graphene oxide directly from nitrogen-doped graphene oxide as a high-performance lithium ion battery anode. RSC Adv. 4 (80), 42412–42417.
Fan, X., Liu, Y., Quan, X., 2019. A novel reduced graphene oxide/carbon nanotube hollow fiber membrane with high forward osmosis performance. Desalination 451, 117–124.
Fernández-Márquez, M., et al., 2022. Improvement of water filtration performance of graphene oxide membranes on Nylon support by UV-assisted reduction treatment: Control of molecular weight cut-off. Chem. Eng. J. 449, 137807.
Goh, P., et al., 2016. Recent trends in membranes and membrane processes for desalination. Desalination 391, 43–60.
Guo, X., et al., 2014. Synthesis of amino functionalized magnetic graphenes composite material and its application to remove Cr (VI), Pb (II), Hg (II), Cd (II) and Ni (II) from contaminated water. J. Hazard. Mater. 278, 211–220.
Han, Y., Xu, Z., Gao, C., 2013. Ultrathin graphene nanofiltration membrane for water purification. Adv. Funct. Mater. 23 (29), 3693–3700.

Haruna, M.A., Wen, D., 2019. Stabilization of polymer nanocomposites in high-temperature and high-salinity brines. ACS Omega 4 (7), 11631–11641.
Homaeigohar, S., Elbahri, M., 2017. Graphene membranes for water desalination. NPG Asia Mater. 9 (8) e427-e427.
Huang, H., Ying, Y., Peng, X., 2014. Graphene oxide nanosheet: an emerging star material for novel separation membranes. J. Mater. Chem. A 2 (34), 13772–13782.
Huang, L., et al., 2013a. Novel hydrophilic nylon 6, 6 microfiltration membrane supported thin film composite membranes for engineered osmosis. J. Membr. Sci. 437, 141–149.
Huang, H., et al., 2013b. Ultrafast viscous water flow through nanostrand-channelled graphene oxide membranes. Nat. Commun. 4 (1), 1–9.
Hu, M., Mi, B., 2013. Enabling graphene oxide nanosheets as water separation membranes. Environ. Sci. Technol. 47 (8), 3715–3723.
Jang, J., et al., 2020. Graphene oxide nanocomposite membrane cooperatively cross-linked by monomer and polymer overcoming the trade-off between flux and rejection in forward osmosis. J. Membr. Sci. 598, 117684.
Jiang, L., Jin, Y., Marcus, R.K., 2015. Polyethylenimine modified poly (ethylene terephthalate) capillary channeled-polymer fibers for anion exchange chromatography of proteins. J. Chromatogr. A 1410, 200–209.
Jia, Z., Wang, Y., 2015. Covalently crosslinked graphene oxide membranes by esterification reactions for ions separation. J. Mater. Chem. A 3 (8), 4405–4412.
Johnson, D.J., Hilal, N., 2020. Can graphene and graphene oxide materials revolutionise desalination processes? Desalination, 114852.
Jusoh, W.Z.A.W., et al., 2019. Fabrication and characterisation of a polyamide thin-film composite membrane on a nylon 6, 6 substrate for isopropanol dehydration. Comptes Rendus Chim. 22 (11–12), 755–760.
Kim, H.W., et al., 2013. Selective gas transport through few-layered graphene and graphene oxide membranes. Science 342 (6154), 91–95.
Kim, S., et al., 2017. Highly crosslinked, chlorine tolerant polymer network entwined graphene oxide membrane for water desalination. J. Mater. Chem. A 5 (4), 1533–1540.
Kuo, W.-S., et al., 2020. Amino-functionalized nitrogen-doped graphene quantum dots for efficient enhancement of two-photon-excitation photodynamic therapy: functionalized nitrogen as a bactericidal and contrast agent. Int. J. Nanomed. 6961–6973.
Kyzas, G.Z., Deliyanni, E.A., Matis, K.A., 2014. Graphene oxide and its application as an adsorbent for wastewater treatment. J. Chem. Technol. Biotechnol. 89 (2), 196–205.
Lim, M.-Y., et al., 2017. Cross-linked graphene oxide membrane having high ion selectivity and antibacterial activity prepared using tannic acid-functionalized graphene oxide and polyethyleneimine. J. Membr. Sci. 521, 1–9.
Lin, Z., et al., 2010. Solvent-assisted thermal reduction of graphite oxide. J. Phys. Chem. C 114 (35), 14819–14825.
Liu, H., et al., 2013. In situ synthesis of the reduced graphene oxide–polyethyleneimine composite and its gas barrier properties. J. Mater. Chem. a 1 (11), 3739–3746.
Liu, H., Wang, H., Zhang, X., 2015. Facile fabrication of free-standing ultrathin reduced graphene oxide membranes for water purification. Adv. Mater. 27 (2), 249–254.
Li, X., Cai, T., Chung, T.-S., 2014. Anti-fouling behavior of hyperbranched polyglycerol-grafted poly (ether sulfone) hollow fiber membranes for osmotic power generation. Environ. Sci. Technol. 48 (16), 9898–9907.
Li, L., Shi, W., Yu, S., 2020. Research on Forward Osmosis Membrane Technology Still Needs Improvement in Water Recovery and Wastewater Treatment. Water 12 (1), 107.
Li, P., et al., 2019a. Preparation of modified graphene oxide/polyethyleneimine film with enhanced hydrogen barrier properties by reactive layer-by-layer self-assembly. Compos. Part B: Eng. 166, 663–672.
Li, N.N., et al., 2011. Advanced Membrane Technology and Applications. John Wiley & Sons.
Li, Z., et al., 2019b. Graphene oxide incorporated forward osmosis membranes with enhanced desalination performance and chlorine resistance. Front. Chem. **7**.
Lv, Y., et al., 2018. Co-deposition kinetics of polydopamine/polyethyleneimine coatings: effects of solution composition and substrate surface. Langmuir 34 (44), 13123–13131.
Maleki, A., et al., 2017. Amine functionalized multi-walled carbon nanotubes: single and binary systems for high capacity dye removal. Chem. Eng. J. 313, 826–835.
McCutcheon, J.R., Elimelech, M., 2006. Influence of concentrative and dilutive internal concentration polarization on flux behavior in forward osmosis. J. Membr. Sci. 284 (1–2), 237–247.
Ndiaye, I., Vaudreuil, S., Bounahmidi, T., 2019. Forward osmosis process: state-of-the-art of membranes. Sep. Purif. Rev. 1–21.
Nxumalo, E.N., Coville, N.J., 2010. Nitrogen doped carbon nanotubes from organometallic compounds: a review. Materials 3 (3), 2141–2171.
Padmavathy, N., et al., 2019. Interlocked graphene oxide provides narrow channels for effective water desalination through forward osmosis. ACS Appl. Mater. Interfaces 11 (7), 7566–7575.
Pang, J., et al., 2019. Exploring the sandwich antibacterial membranes based on UiO-66/graphene oxide for forward osmosis performance. Carbon 144, 321–332.
Parsamehr, P.S., et al., 2019. Preparation of novel cross-linked graphene oxide membrane for desalination applications using (EDC and NHS)-activated graphene oxide and PEI. Desalination 468, 114079.
Qiao, X., et al., 2015. Phosphorus and nitrogen dual doped and simultaneously reduced graphene oxide with high surface area as efficient metal-free electrocatalyst for oxygen reduction. Catalysts 5 (2), 981–991.
Roy, S., Kim, J., 2019. Synergistic effect of polydopamine–polyethylenimine copolymer coating on graphene oxide for EVA nanocomposites and high-performance triboelectric nanogenerators. Nanoscale Adv. 1 (6), 2444–2453.
Sahebi, S., et al., 2017. Thin-film composite membrane on a compacted woven backing fabric for pressure assisted osmosis. Desalination 406, 98–108.
Song, J.-h, et al., 2019. Tuning the nanostructure of nitrogen-doped graphene laminates for forward osmosis desalination. Nanoscale 11 (45), 22025–22032.
Song, J., Wang, X., Chang, C.-T., 2014. Preparation and characterization of graphene oxide. J. Nanomater. **2014**.
Stankovich, S., et al., 2007. Synthesis of graphene-based nanosheets via chemical reduction of exfoliated graphite oxide. carbon 45 (7), 1558–1565.
Sui, Z.-Y., et al., 2013. Preparation of three-dimensional graphene oxide–polyethylenimine porous materials as dye and gas adsorbents. ACS Appl. Mater. Interfaces 5 (18), 9172–9179.
Suk, J.W., et al., 2010. Mechanical properties of monolayer graphene oxide. ACS Nano 4 (11), 6557–6564.
Talar, A.J., et al., 2019. Investigation on effect of KCl addition on desalination performance of co-polymerized GO/Nylon nanocomposite membrane. Process Saf. Environ. Prot. 125, 31–38.
Tiraferri, A., et al., 2013. A method for the simultaneous determination of transport and structural parameters of forward osmosis membranes. J. Membr. Sci. 444, 523–538.
Tiwari, S., Gogoi, A., Reddy, K.A.J.P.C.C.P., 2019. What governs the nature of fouling in forward osmosis (FO) and reverse osmosis (RO)? A molecular dynamics study. 21 (43), 24165–24176.
Tuinstra, F., Koenig, J.L., 1970. Raman spectrum of graphite. J. Chem. Phys. 53 (3), 1126–1130.
Wang, L., et al., *Sandwich layered double hydroxides with graphene oxide for enhanced water desalination*. 2022. **65**(3): p. 803–810.
Wang, L., et al., 2014. Aqueous phase synthesis of highly luminescent, nitrogen-doped carbon dots and their application as bioimaging agents. Langmuir 30 (47), 14270–14275.

Wang, R., et al., 2013. Facile one-step hydrazine-assisted solvothermal synthesis of nitrogen-doped reduced graphene oxide: reduction effect and mechanisms. RSC Adv. 3 (4), 1194–1200.
Wang, Z., et al., 2015. Mussel-inspired hybrid coatings that transform membrane hydrophobicity into high hydrophilicity and underwater superoleophobicity for oil-in-water emulsion separation. ACS Appl. Mater. Interfaces 7 (18), 9534–9545.
Wu, W., et al., 2020. Recent development of graphene oxide based forward osmosis membrane for water treatment: A critical review. Desalination 491, 114452.
Xu, K., et al., 2016. Synthesis of highly stable graphene oxide membranes on polydopamine functionalized supports for seawater desalination. Chem. Eng. Sci. 146, 159–165.
Yan, Y., et al., 2017a. A graphene-like membrane with an ultrahigh water flux for desalination. Nanoscale 9 (47), 18951–18958.
Yan, F., et al., 2017b. Preparation of freestanding graphene-based laminar membrane for clean-water intake via forward osmosis process. RSC Adv. 7 (3), 1326–1335.
Yang, E., et al., 2017. Enhanced desalination performance of forward osmosis membranes based on reduced graphene oxide laminates coated with hydrophilic polydopamine. Carbon 117, 293–300.
Yang, E., et al., 2018. Laminar reduced graphene oxide membrane modified with silver nanoparticle-polydopamine for water/ion separation and biofouling resistance enhancement. Desalination 426, 21–31.
Yuan, Y., et al., 2017. Enhanced desalination performance of carboxyl functionalized graphene oxide nanofiltration membranes. Desalination 405, 29–39.
Zhang, Y., Chung, T.-S., 2017. Graphene oxide membranes for nanofiltration. Curr. Opin. Chem. Eng. 16, 9–15.
Zhang, Y., Zhang, S., Chung, T.-S., 2015. Nanometric graphene oxide framework membranes with enhanced heavy metal removal via nanofiltration. Environ. Sci. Technol. 49 (16), 10235–10242.
Zhang, B., et al., 2012. Preparation of polymer decorated graphene oxide by γ-ray induced graft polymerization. Nanoscale 4 (5), 1742–1748.
Zhao, S., et al., 2012. Recent developments in forward osmosis: opportunities and challenges. J. Membr. Sci. 396, 1–21.
Zheng, S., et al., 2017. Swelling of graphene oxide membranes in aqueous solution: characterization of interlayer spacing and insight into water transport mechanisms. ACS Nano 11 (6), 6440–6450.
Zhou, X., et al., 2015. The carbonization of polyethyleneimine: facile fabrication of N-doped graphene oxide and graphene quantum dots. RSC Adv. 5 (128), 105855–105861.